# A Cross-Validation Approach to Approximate Basis Function Selection of the Stall Flutter Response of a Rectangular Wing in a Wind Tunnel

Sunil L. Kukreja*
*NASA Dryden Flight Research Center, Edwards, California 93523*
Gareth A. Vio†
*The University of Sydney, NSW 2006, Australia*
Thomas Andrianne‡ , Norizham Abdul Razak ‡ and Grigorios Dimitriadis ‡
*University of Liège, Liège 4000, Belgium*

**The stall flutter response of a rectangular wing in a low speed wind tunnel is modelled using a nonlinear difference equation description. Static and dynamic tests are used to select a suitable model structure and basis function. Bifurcation criteria such as the Hopf condition and vibration amplitude variation with airspeed were used to ensure the model was representative of experimentally measured stall flutter phenomena. Dynamic test data were used to estimate model parameters and estimate an approximate basis function.**

## I. Introduction

The existence of nonlinearities in aeroelastic systems is known to significantly affect their dynamic behavior, often inducing oscillations that cannot be predicted by linear theory.[1] One such type of oscillation is known as stall flutter.[2] Traditionally, aeroelastic phenomena are considered to be dynamic responses resulting from interaction of structural, inertial and aerodynamic forces. Such interactions can lead to the well-known classical linear flutter, a catastrophic self-excited oscillation.[3] However, several other incidents can arise from low speed aeroelastic interactions, such as stall flutter and galloping,[4] which are due to the presence of an underlying nonlinearity in the aerodynamic forces. These events frequently lead to Limit Cycle Oscillations (LCO). LCOs also result from other sources, such as structural or material nonlinearities.

Stall flutter is a phenomenon that occurs when flow separates from and reattaches to the surface of a wing in a cyclic manner. The separation can be partial or complete over the entire wing's surface. This alternation between stalled and attached flow is known as dynamic stall, a phenomenon that has been the subject of numerous experimental and theoretical investigations (see for example McCroskey et al,[5] Ericsson and Reding[6] and Spentzos et al[7]). Stall flutter is the result of coupling of the vibration characteristics of a flexible structure with dynamic stall.[8]

Historically, several simple models of stall flutter have been developed, such as those by Ericsson.[8] However, practically such models are quasi-steady, i.e. they are derived from steady lift and pitching moment curves of a wing. In the present work, a straightforward mathematical model of stall flutter is developed from measurement of dynamic responses. Abdul Razak et al[9,10] conducted a set of experiments on a rectangular wing in a low speed wind tunnel that underwent stall flutter in pitch. These experiments are used to identify a nonlinear discrete-time model of stall flutter response of a wing and estimate the fundamental parameters of its dynamics and static function.

The model was estimated using a cross-validation approach.[11,12] Model development via cross-validation is concerned with assessing whether a given nominal model can reproduce data from a plant, collected after

*Structural Dynamics Group, Aerostructures Branch, MailStop T-47.
†School of Aerospace, Mechanical and Mechatronic Engineering, J07.
‡Aerospace and Mechanical Engineering Department, B52 Chemin des chevreuils 1.

some initial experiments to obtain estimation data.[13] The model validation problem is really one of model invalidation since a given model can only be said to be not invalidated with the current evidence. Future evidence may invalidate the model.

The motivation for this study is to investigate whether an approximate basis function can be parameterized and estimated using the $\ell_2$ estimator, thus, avoiding a nonlinear least-squares estimation and search paradigm. While this work provides an ad-hoc approach to basis function parameterization it is not a replacement for the traditional nonlinear least-squares approach. This work offers a coarse estimation, which may be adequate in most applications or provide a possible seeding for nonlinear search techniques such as the well-known Levenberg-Marquardt algorithm.[14,15,16]

## II. Experiment Description

Below we provide details of the experimental testbed and procedures used for data collection and analysis to obtain a basis function class.

### A. Support System

The experiments[9,10] were conducted in the Multi-Disciplinary Low Speed Wind Tunnel of the University of Liège. The wind tunnel features two working sections, one for aeronautical and automotive applications and one for wind engineering applications. Experiments were carried out in the aeronautical working section, which has dimensions of 2m $\times$ 1.5m $\times$ 5m (width $\times$ height $\times$ length) and is capable of achieving airspeeds of up to 60 m/s in the tunnel's closed loop configuration. The turbulence level was 0.15% on average at lower speed ranges. For stall flutter experiments a special support framework was assembled, which was used to fix extension springs. Ends of the springs were fixed to arms that acted as adaptors to the wing spar. The spar was connected to the center of the arm. Free-play was avoided by securely attaching the spar to the adaptor arms. The suspension springs allowed movement in all directions. The support mechanism described was designed to allow frictionless wing vibrations with known structural stiffness values. Eight to sixteen springs can be installed to suspend a wing and keep it in tension. Even numbers of springs were used to ensure symmetry in stiffness. The complete support system is shown in Fig. 1.

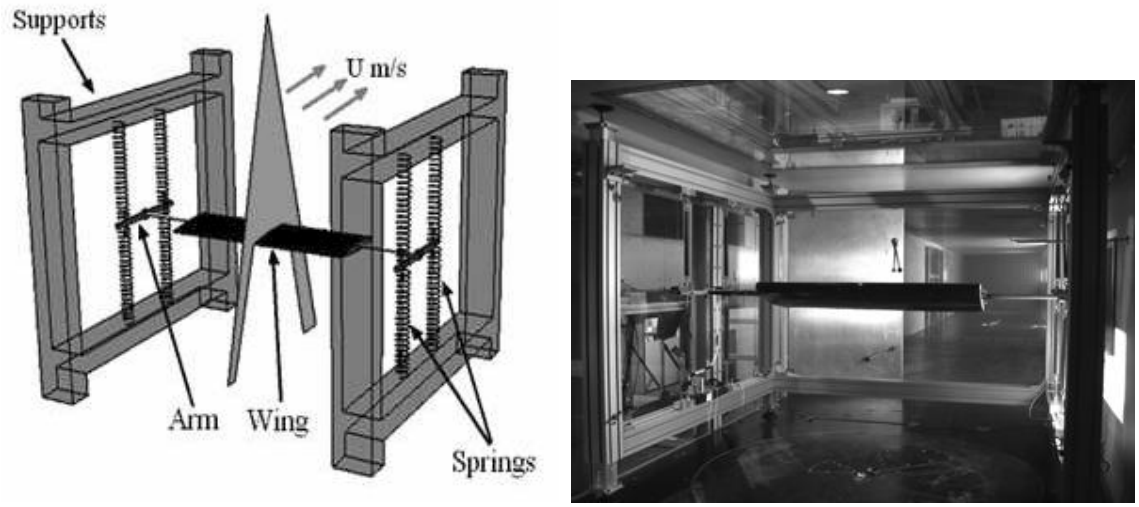


(a) Drawing (b) Photograph in wind tunnel

**Figure 1. Wing and support design and construction**

### B. Wing

A rigid straight rectangular wing was constructed from aluminum and balsa wood. The wing chord was 36.0 cm long and span 100 cm, resulting in an aspect ratio of 2.78. The skin consisted of a 0.5 mm thick aluminum sheet that was wrapped around balsa ribs. There were six ribs inside the wing, positioned 18.0

cm apart. The 2.0 cm thick ribs were held together by an aluminum rod acting as a main spar, located at 37% of the chord. The airfoil selected for this study was the NACA 0018. This thickness ratio was chosen for two reasons. Firstly, it was high enough to allow the installation of instrumentation inside the wing. Secondly, it was thicker than the NACA 0012 airfoil investigated by Dimitriadis and Li.[17] It was hoped that the increased thickness would give rise to different stall phenomena. This design allowed ballast to be attached internally. Mass of the wing including main spar, adaptor arms and instrumentation was 6.47 kg and its spring stiffness was 755 N/m.

To measure the unsteady pressure distribution, 16 pressure tappings were drilled on the wing surface, at the mid-span point. These tappings were connected to 16 piezoresistive pressure transducers[18] by means of plastic tubes.[19] They were positioned symmetrically on the wing's upper and lower surfaces, as shown in Fig. 2. The phase lags associated with the tubes were discussed in.[18]

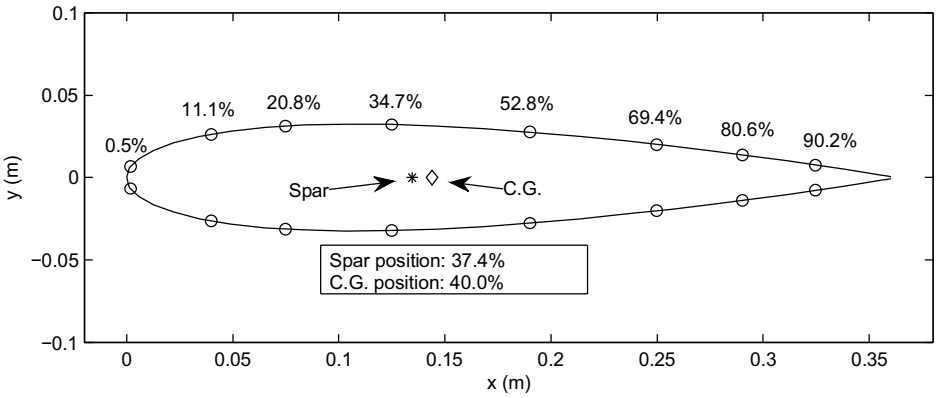


**Figure 2. Position of pressure sensors, spar and center of gravity relative to the wing section**

Wing motion was measured using four accelerometers attached on the spring adaptor arms. Their frequency measurement range was between 0-300 Hz with accuracy of ±5% and their measurement range is ±50 g. The pressure sensors and accelerometers were sampled at 1.0 kHz using a National Instruments PXI 1010 data acquisition module managed by Labview 9 software. From these measurements, pitch and plunge displacements of the wing were reconstructed by numerically integrating acceleration values twice. There were no end-plates attached to the wingtips to allow good quality flow visualization could be obtained. As a result, flow over the wing was three-dimensional.

### C. Procedure

Two parameters varied during these experiments are as follows:

- Wind tunnel airspeed, $V$ (from 0 m/s to a maximum of 26 m/s)
- Wind-off static pitch angle, $\alpha_0$ (from 11° to 16°)

Experimental procedure consisted of setting the wind-off static pitch angle then gradually increasing airspeed. At each new airspeed, when wing response was stabilised, 4 seconds of acceleration and pressure response data was recorded. No external excitation was applied besides the natural turbulence of the wind tunnel.

Before starting the wind-on tests, wind-off instrumented hammer tests were performed in order to determine the natural frequencies of the degrees of freedom of the wing. The frequency values for the plunge, pitch and roll degrees of freedom are tabulated in Table 1. The yaw, lateral translation and longitudinal degrees of freedom have higher natural frequencies.

### D. Data Analysis

Accelerometer data were first analysed to obtain pitch, plunge and roll accelerations. These responses were band-pass filtered between 2Hz and 80Hz, using a rectangular frequency domain filter. They were then

| Mode | Frequency | Damping ratio |
|---|---|---|
| Plunge | 4.57Hz | 0.0033 |
| Pitch | 5.95Hz | 0.0087 |
| Roll | 13.10Hz | 0.0418 |

**Table 1. Natural frequencies and dampings at $U = 0$ m/s**

integrated in time twice to estimate the pitch, plunge and roll velocities and displacements. Integration was carried out in the time domain using a central difference scheme.

Pressure data were integrated around the wing's central section to obtain sectional aerodynamic lift and moment coefficients. These signals were band-pass filtered between 2Hz and 80Hz. Note that lift and moment coefficients are sectional and, therefore, do not represent the total lift and moment acting on the wing. In this work, the sectional moment coefficient is used to choose a basis function for identification of the wing's response. This choice is based on variation of sectional lift and moment coefficient values with pitch displacement and velocity responses.

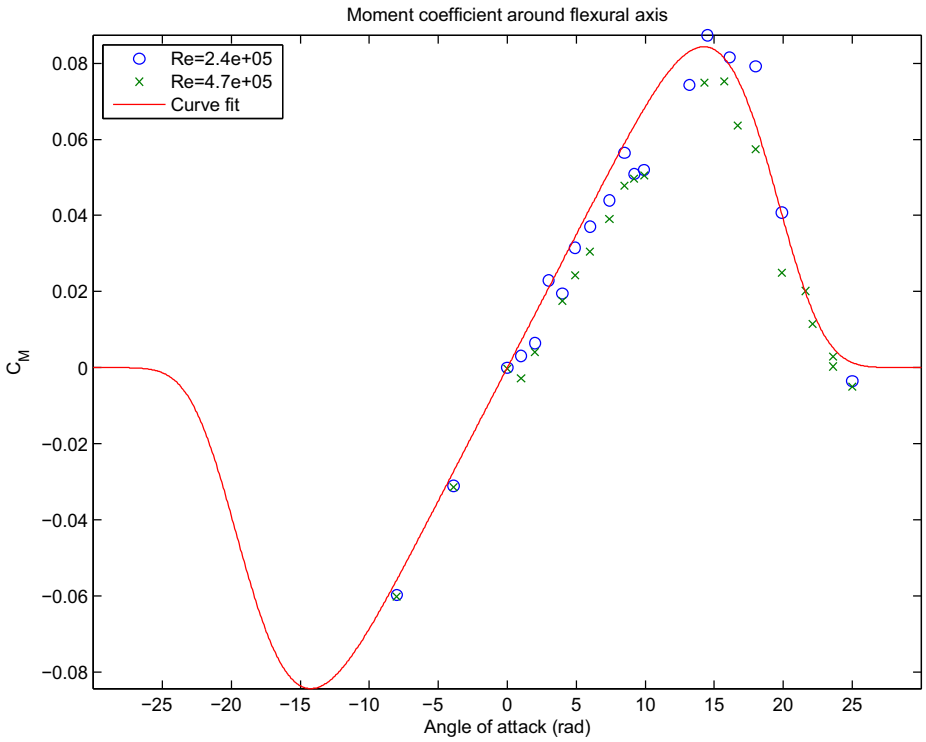


**Figure 3. Static pitching moment variation with angle of attack at two different Reynolds numbers.**

## III. Results

Only a subset of the experimental results is presented in this work. For a more complete description see Abdul Razak et al.[10] Static aerodynamic pitching moment results are presented first, followed by dynamic responses.

### A. Static Results

Figure 3 shows the total static aerodynamic pitching moment coefficient variation around the pitching axis with pitch angle. The data shown in the figure were obtained using a force and moment balance setup. The

wing was placed at different pitch angles and its total lift and drag were measured using six force gauges; aerodynamic moment around the pitching axis was measured using a single torque gauge. Static experiments were repeated at two Reynolds numbers representative of subsequent dynamic experiments. The pitching moment coefficient is defined as

$$c_m = \frac{m}{1/2\rho V^2 Sc} \tag{1}$$

where $m$ is the pitching moment, $\rho$ is the air density, $V$ is the wind tunnel airspeed, $S$ the wing surface area and $c$ is the chord of the wing.

Figure 3 illustrates that the moment curve is linear up to a pitch angle of approximately $14^\circ$. Nose up pitching moments are defined as positive and, hence, the effect of the pitching moment is destabilising. At pitch angles higher than the linear limit the pitching moment becomes less destabilising.

The static pitching moment coefficient data can be curve-fitted using a function of the form

$$c_m = h_1 \alpha \exp\left(-h_2 \alpha^{h_3}\right) \tag{2}$$

where $c_m$ is the non-dimensional aerodynamic pitching moment coefficient and $\alpha$ is the pitch angle. Note that Fig. 3 plots a curve-fit based on Eqn. 2, where $h_1 = 0.4011$, $h_2 = 707.5641$, $h_3 = 6$ and $\alpha$ is in rad. The curve-fit provides a good approximation up to pitch angles of $24^\circ$.

Since pitch responses were obtained from integrating acceleration signals, the mean values of these responses were lost. However, mean data can be reconstructed using the results in Fig. 3. It is assumed that the mean value of pitch response is equal to the static deformation of the wing's pitch angle at the same airspeed. This deformation is given by the static equilibrium equation

$$k_\alpha(\alpha_e - \alpha_0) = \frac{1}{2}\rho V^2 Sc \; c_{m_{static}}(\alpha_e) \tag{3}$$

where $k_\alpha$ is wing stiffness in the pitch degree of freedom, $\alpha_e$ is mean pitch angle at airspeed $V$ and $\alpha_0$ is wind-off pitch angle. This equation is nonlinear but can be solved iteratively or graphically.

### B. Dynamic Results

Dynamic tests were performed after the static tests, replacing the force balance setup with the spring assembly shown in Fig. 1. For all selected wind-off static pitch angles, at low airspeeds the response was noisy and of low amplitude. For a static pitch angle of $11^\circ$, significant high amplitude vibrations occurred at airspeeds higher than 25 m/s. This is a classical flutter phenomenon. The highest airspeed tested was limited to 25.5 m/s for safety reasons.

For the other static pitch angles, lower amplitude vibrations were encountered at lower airspeeds. Vibrations occurred primarily in pitch degree of freedom, with very little motion in other degrees of freedom. The amplitude of these vibrations increased gradually with airspeed, particularly for the highest static pitch angles of $14^\circ - 16^\circ$. Figure 4 shows variation of pitch angle response amplitude with airspeed for all tested angles of attack.

## IV. Discrete-Time Nonlinear Model Representation

In this work, the construction of identified models describing the stall flutter response of a wing is considered. Therefore, low amplitude responses to turbulence at low airspeeds and the classical flutter phenomenon at $\alpha_0 = 11^\circ$ is ignored. As mentioned previously, stall flutter responses predominantly involve pitch degree of freedom. Therefore, the phenomenon can be modelled as a single degree of freedom vibration. The equation of motion for the wing can be written as

$$I_\alpha \ddot{\alpha}(t) + c_\alpha \dot{\alpha}(t) + k_\alpha \alpha(t) = \frac{1}{2}\rho V^2 Sc \; c_m(\alpha(t_1), \dot{\alpha}(t_1), \ddot{\alpha}(t_1)) \tag{4}$$

where $t$ is time, $\alpha$ is pitch angle, $I_\alpha$ is wing's moment of inertia around the pitch axis, $c_\alpha$ is wing structural damping in the pitch degree of freedom, $\rho$ is air density and $c$ is wing chord length. In Eqn. 4, the pitching moment coefficient is expressed as a nonlinear function of the current and past values of system states. The motion started at time $t = 0$, and $t_1$ takes values from 0 to $t$. Dependence on past values of system states reflects the well-known property of infinite dimensionality of unsteady aerodynamics.

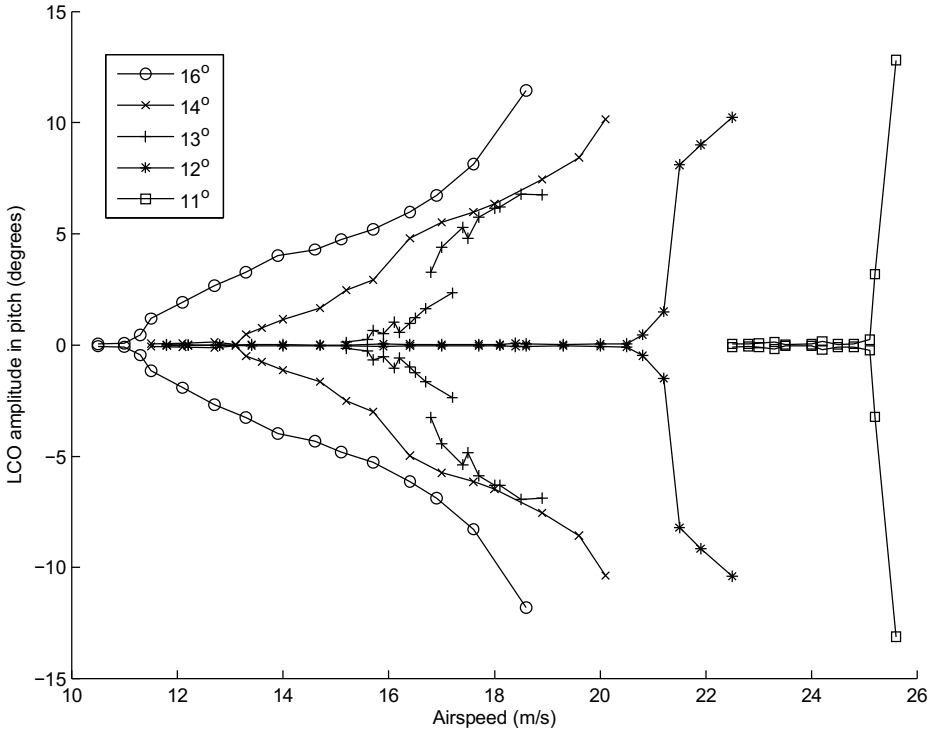


**Figure 4. Pitch response amplitudes at all angles of attack and airspeeds**

Equation 4 can be simplified if it is assumed that the added mass effect is small compared to the moment of inertia of the wing's structure, even when flow is stalled. In this case, Eqn. 4 becomes

$$I_\alpha \ddot{\alpha}(t) + c_\alpha \dot{\alpha}(t) + k_\alpha \alpha(t) = \frac{1}{2}\rho V^2 Sc \; c_m(\alpha(t_1), \dot{\alpha}(t_1)) \tag{5}$$

To reflect experimental conditions in the wind tunnel, an additional excitation force term can be added to model the effect of free stream turbulence. If it is assumed that this effect is much smaller than the self-excited stall flutter oscillations, the equation of motion can be written as

$$I_\alpha \ddot{\alpha}(t) + c_\alpha \dot{\alpha}(t) + k_\alpha \dot{\alpha}(t) = \frac{1}{2}\rho V^2 Sc \; c_m(\alpha(t_1), \dot{\alpha}(t_1)) + f(t) \tag{6}$$

where $f(t)$ is a random excitation force of small amplitude.

### A. Nonlinear Structure of Moment Coefficient

Using the present approach, the moment coefficient is an unknown nonlinear function of pitch displacement and velocity at all times since the onset of motion. To choose an approximate basis and model form for this nonlinear system, sectional pitching moment coefficient signals measured using the pressure tappings were utilized. These signals do not represent a complete 3D aerodynamic pitching moment acting on the wing. However, it is assumed that the sectional moment coefficient has the same nonlinear form as the 3D moment coefficient and, therefore, can be used to provide a good approximation.

Figure 5(a) shows the time response of $\alpha$, $\dot{\alpha}$ and $c_m$ for $\alpha_0 = 14^\circ$ and $V = 11.5$ m/s. The oscillation amplitudes are very small (less than $1^\circ$ in pitch displacement) and the signals feature significant randomness. Figure 5(a) depicts a typical response to the wind tunnel's free stream turbulence, in the absence of any self-excited phenomena. Figure 5(b) displays $c_m$ on the $z$-axis against $\alpha$ and $\dot{\alpha}$ on the $x$ and $y$ axes, respectively. This plot is very messy and without any clear structure.

By contrast, Fig. 6 shows the time response and phase plane plots at the same wind-off pitch angle but a higher airspeed, $V = 20.1$ m/s. In this case, the signals are significantly more ordered and have

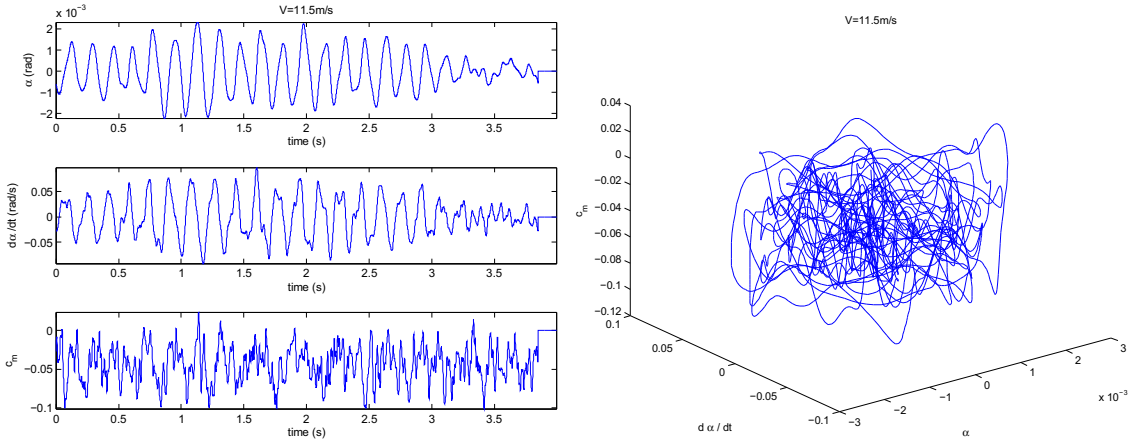


(a) Time responses (b) Phase plane

**Figure 5. Time responses and phase plane plots of $\alpha$, $\dot{\alpha}$ and $c_m$ at low airspeed**

a single principal frequency component. Nevertheless, the moment coefficient varies more stochastically than pitch displacement and velocity responses. This phenomenon is due to the fact that the separation and reattachment of the boundary layer are quasi-repeatable processes. During each cycle, separation and reattachment occur at slightly different phase values. As a consequence, the phase plot of Fig. 6(b) is noisy but has a clear structure. Furthermore, it is repeatable within some confidence bounds.

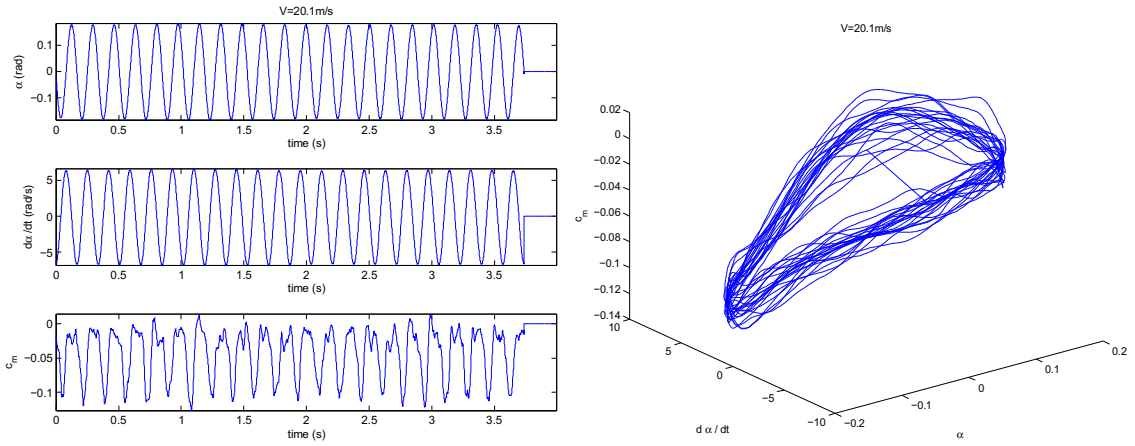


(a) Time responses (b) Phase plane

**Figure 6. Time responses and phase plane plots of $\alpha$, $\dot{\alpha}$ and $c_m$ at high airspeed**

The objective of this section is to develop a discrete-time model representation for $c_m$, which is capable of representing phase-plane plots such as Fig. 6(b). If no nonlinearity exists or the system is perturbed around a sufficiently small operating point, an ARMA (Auto-Regressive Moving Average) model structure would suffice and is represented as,

$$c_m(n) = \gamma_0\alpha(n) + \gamma_1\alpha(n-1) + \gamma_2\alpha(n-2) + \ldots + e(n) + \delta_1 e(n-1) + \delta_2 e(n-2)\ldots \tag{7}$$

where $n$ is a discrete-time instance, $e(n)$ is a noise sequence and $\gamma_i$, $\delta_i$ are coefficients to be estimated. However, such a model cannot represent the correct geometric shape of the manifold in Fig. 6(b) and will result in a linear model for the entire wing that is incapable of predicting LCOs. Therefore, a nonlinear model must be formulated.

To choose an appropriate nonlinear model structure for the manifold of Fig. 6(b), it is observed that the plot is a 3D curve. However, if the manifold is rotated appropriately, it can be seen that it lies on a curved

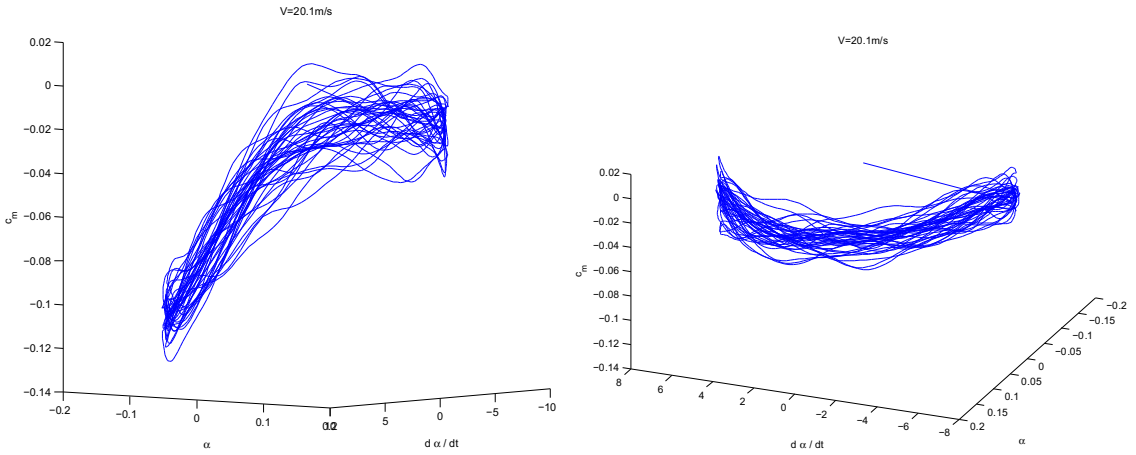


(a) Az=-40°, El=-4°

(b) Az=-112°, El=-34°

**Figure 7. Figure 6(b) plotted at different azimuth and elevation angles**

2D plane . Figure 7 shows the same manifold at two different sets of azimuth and elevation angles. This illustrates that for two combinations of azimuth and elevation, the manifold is an approximately 2D curve. This phenomenon is common to all measured LCOs, although rotation angles differ for each case. Notice that the plot in Fig. 7(a) resembles the static pitching moment curve in Fig. 3 at pitch angles between 10° and 20°. Therefore, to obtain an estimate of $c_m$, the cycle $\dot{\alpha}(\alpha)$ can be mapped onto a curved plane, as shown in Fig. 8. The shape of the plane is inspired by the function used to curve fit the static pitching moment coefficient data, as shown in Eqn. 2. The coordinates of that plane are given by

$$\mathbf{x} = \mathbf{R}\mathbf{R}_z \begin{pmatrix} \alpha/w_x \\ \dot{\alpha}/w_y \\ -\alpha \exp\left(-\alpha^4/w_w\right)/w_z \end{pmatrix} + b\mathbf{v} \tag{8}$$

where $\mathbf{x} = [x \quad y \quad z]^T$ are coordinates of the mapping plane in $\alpha$-$\dot{\alpha}$-$c_m$ space, $w_x$, $w_y$ and $w_z$ are normalisation coefficients, $b$ is a displacement coefficient and $\mathbf{v}$ is a unit vector perpendicular to the direction of the curvature of the plane, given by

$$\mathbf{v} = [\cos\phi \quad \sin\phi \quad 0]^T \tag{9}$$

where $\phi$ is the azimuth angle that collapses the $c_m$ manifold into a 2D curve, in this case $-40°$ as in Fig. 7(a). $\mathbf{R}_z$ is the azimuthal rotation matrix given by

$$\mathbf{R}_z = \begin{pmatrix} \cos\phi & -\sin\phi & 0 \\ \sin\phi & \cos\phi & 0 \\ 0 & 0 & 1 \end{pmatrix} \tag{10}$$

and $\mathbf{R}$ rotates the mapping plane around an axis aligned with $\mathbf{v}$ by an angle equal to the elevation angle $\psi$ required to collapse the $c_m$ manifold to two dimensions, in this case $-4°$. $\mathbf{R}$ is given by

$$\mathbf{R} = \begin{pmatrix} \cos\psi + \cos^2\phi^2(1-\cos\psi) & \cos\phi\sin\phi(1-\cos\psi) & \sin\phi\sin\psi \\ \cos\phi\sin\phi(1-\cos\psi) & \cos\psi + \sin^2\phi(1-\cos\psi) & \cos\phi\sin\psi \\ -\sin\phi\sin\psi & \cos\phi\sin\psi & \cos\psi \end{pmatrix} \tag{11}$$

From Eqn. 8, it is clear that a good approximation of the geometric plane on which $c_m$ lies has been obtained by means of a simple nonlinear function. Note that in the case of Eqn. 8 the exponent of $\alpha$ inside the exponential is 4 as opposed to 6 in the static pitching moment case. In the sequel, a generalized form of this basis function is used to develop a robust model description.

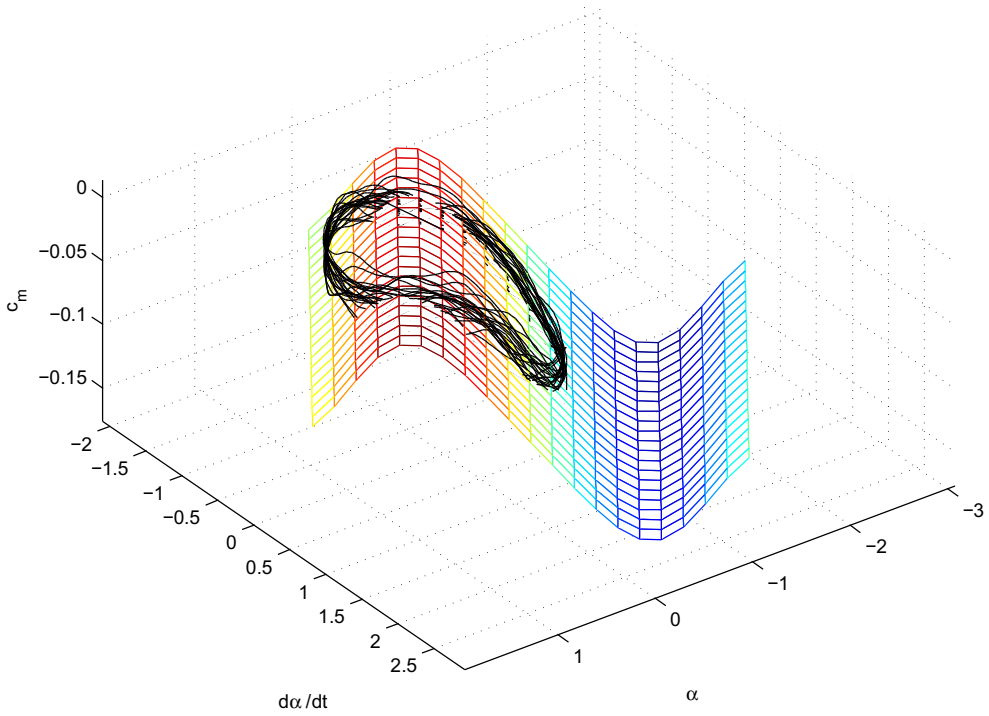


**Figure 8. Moment coefficient manifold and mapping plane**

## B. Constraints

The nonlinear function $c_m$ must satisfy some known constraints. First, the system undergoes a Hopf Bifurcation at a critical airspeed, $V_c$, such that a periodic solution branch appears in the system's bifurcation diagram at that airspeed. For a single degree of freedom system of the form of Eqn. 5 or 6, the Hopf bifurcation can be described by considering stability of the equilibrium solution $\alpha = \alpha_e$. The stability of this solution is identical to the stability of the linear system

$$I_\alpha \ddot{\alpha}(t) + c_\alpha \dot{\alpha}(t) + k_\alpha \alpha(t) = \frac{1}{2}\rho V^2 Sc \left( \left.\frac{\partial c_m}{\partial \alpha}\right|_{\alpha_e, V} \alpha + \left.\frac{\partial c_m}{\partial \dot{\alpha}}\right|_{\alpha_e, V} \dot{\alpha} \right) \tag{12}$$

For a Hopf bifurcation to occur, total damping of the linear system above must be equal to zero. This yields a bifurcation condition for the form

$$\left.\frac{\partial c_m}{\partial \dot{\alpha}}\right|_{\alpha_e, V_c} = \frac{2c_\alpha}{\rho V_c^2 Sc} \tag{13}$$

Second, the nonlinearity must satisfy the limit cycle amplitude and fundamental frequency. At airspeeds higher than the bifurcation airspeed the system undergoes LCOs whose amplitude and frequency have been measured. Therefore, the nonlinearity must be capable of matching these measured values. To describe this condition, a first order Harmonic Balance expansion is applied to the equation of motion. It is assumed that the LCO response of the nonlinear equation of motion can be written as

$$\alpha(t) = A \sin \omega t \tag{14}$$

where $A$ is LCO amplitude and $\omega$ is frequency. Substituting this solution into the equation of motion yields

$$-A\omega^2 I_\alpha \sin \omega t + A\omega c_\alpha \cos \omega t + A k_\alpha \sin \omega t = \frac{1}{2}\rho V^2 Sc (a_0 + a_1 \cos \omega t + b_1 \sin \omega t) \tag{15}$$

where $a_0$, $a_1$ and $b_1$ are coefficients of a Fourier series given by

$$a_0 = \frac{\omega}{\pi} \int_0^{2\pi/\omega} c_m \left(A \sin \omega t, A \cos \omega t\right) dt$$

$$
\begin{aligned}
a_1 &= \frac{\omega}{\pi}\int_0^{2\pi/\omega} c_m\left(A\sin\omega t, A\cos\omega t\right)\cos\omega t dt \\
b_1 &= \frac{\omega}{\pi}\int_0^{2\pi/\omega} c_m\left(A\sin\omega t, A\cos\omega t\right)\sin\omega t dt.
\end{aligned}
$$

Substituting into Eqn. 15 and carrying out harmonic balancing yields

$$
\begin{aligned}
\int_0^{2\pi/\omega} c_m\left(A\sin\omega t, A\cos\omega t\right) dt &= \frac{2\pi\alpha_e}{\rho V^2 Sc\omega} \\
\int_0^{2\pi/\omega} c_m\left(A\sin\omega t, A\cos\omega t\right)\sin\omega t dt &= \frac{2\pi A}{\rho V^2 Sc\omega}\left(-\omega^2 I_\alpha + k_\alpha\right) \\
\int_0^{2\pi/\omega} c_m\left(A\sin\omega t, A\cos\omega t\right)\cos\omega t dt &= \frac{2\pi A}{\rho V^2 Sc\omega} c_\alpha
\end{aligned}
\tag{16}
$$

Conditions 13 and 16 can be used in order to select a suitable set of basis functions for the nonlinear term $c_m$.

### C. Choice of Nonlinear Function

Satisfying the constraints above yields a suitable form of nonlinear function $c_m$ represented as

$$
c_m = p_1\alpha\exp\left(-p_2\alpha^{p_3}\right) + p_4\frac{\dot{\alpha}}{V}. \tag{17}
$$

The linear term in $\dot{\alpha}$ is necessary to satisfy condition 13. Nevertheless, this model is restrictive because the exponent $p_3$ must be an even integer, if the function is to remain real and finite at negative values of $\alpha$. A generalization of the model, that allows odd and non-integer exponents can be written as

$$
c_m = p_1\alpha\exp\left(-p_2\left|\alpha^{p_3}\right|\right) + p_4\frac{\dot{\alpha}}{V} \tag{18}
$$

where $|\ |$ denotes the absolute value.

### D. Full Model

Using the formulation of Eqn. 18, the equation of motion of the wing in pitch becomes

$$
I_\alpha\ddot{\alpha}(t) + c_\alpha\dot{\alpha}(t) + k_\alpha(\alpha(t)-\alpha_0) = \frac{1}{2}\rho V^2 Sc\ p_1\alpha\exp\left(-p_2\left|\alpha^{p_3}\right|\right) + \frac{1}{2}\rho V^2 Sc\ p_4\frac{\dot{\alpha}}{V} \tag{19}
$$

where the centering of the pitch spring around the wind-off pitch angle is taken into account.

Equation 19 can be posed in discrete-time form using a central difference approximation, centered around time index $n-1$. The pitch acceleration and velocity terms are written as

$$
\begin{aligned}
\ddot{\alpha} &= \frac{\alpha(n) - 2\alpha(n-1) + \alpha(n-2)}{\Delta t^2} \\
\dot{\alpha} &= \frac{\alpha(n) - \alpha(n-2)}{2\Delta t}
\end{aligned}
$$

where the notation $\alpha(n)$ denotes $\alpha(n\Delta t)$ and $\Delta t$ is the time step between two successive experimental measurements, in this case equal to 0.001s. The discrete-time form of the equation of motion is then

$$
\left(\frac{I_\alpha}{\Delta t^2} + \frac{c_\alpha - 1/2\rho V Sc\ p_4}{2\Delta t}\right)\alpha(n) = k_\alpha\alpha_0 + \left(\frac{2I_\alpha}{\Delta t^2} - k_\alpha\right)\alpha(n-1)
$$

$$
+\left(-\frac{I_\alpha}{\Delta t^2} + \frac{c_\alpha - 1/2\rho V Sc\ p_4}{2\Delta t}\right)\alpha(n-2) + \frac{1}{2}\rho V^2 Sc\ p_1\alpha(n-1)\exp\left(-p_2\left|\alpha(n-1)^{p_3}\right|\right). \tag{20}
$$

Wind-off dynamic tests provide values of several coefficients in this formulation, namely, $I_\alpha$, $c_\alpha$ and $k_\alpha$. Furthermore, $p_4$ is known from Eqn. 13, i.e.

$$p_4 = \frac{2c_\alpha}{\rho V_c S c}. \tag{21}$$

The exponent $p_3$ is not known *a priori*. Unfortunately, integrals in the first and second conditions of Eqn. 16 cannot be evaluated analytically. However, they can be evaluated numerically such that

$$\begin{aligned} \sum_{n=0}^{2\pi/\omega\Delta t} p_1 \alpha(n) \exp\left(-p_2 \left|\alpha(n)^{p_3}\right|\right)\Delta t &= \frac{2\pi\alpha_e}{\rho V^2 S c\omega} \\ \sum_{n=0}^{2\pi/\omega\Delta t} p_1 \alpha(n) \exp\left(-p_2 \left|\alpha(n)^{p_3}\right|\right) \sin\left(\omega n\Delta t\right)\Delta t &= \frac{2\pi A}{\rho V^2 S c\omega}\left(-\omega^2 I_\alpha + k_\alpha\right). \end{aligned} \tag{22}$$

Therefore, a complete model of the wing can be obtained by estimating the unknown parameters of Eqn. 20 given the constraints 22.

## V. Best Fit Model via Cross-Validation

Although Eqn. 20 provides a compact model description, it yields a non-trivial estimation problem. A typical estimation procedure would involve a nonlinear least-squares approach because of the unknown coefficients associated with the exponential term.[20] In this paper, we chose to parameterize a set of basis functions using *a priori* knowledge from the present dynamic experiments and using a cross-validation technique to select a best fit model which contains an approximate basis function.

### A. Predicitive Capability Using an ARMA Model Formulation

In many cases although a nonlinear model is suspected or assumed from finite element modelling efforts, experiments are conducted about a small operating region due to safety concerns and hardware limitations. This often renders the nonlinear effect unobservable and, hence, unidentifiable.[21] As such, we first estimate a linear model, namely, Eqn. 20 with the basis function truncated to assess whether a linear model is capable of predicting the observed output before proceeding to postulate a more advanced nonlinear one.

Specifically, we used one of eleven datasets for estimation and the remaining ten to validate the linear model's predictive capability. The accuracy of a $k$-step-ahead predictor was quantified by computing the %Fit as

$$\%\text{Fit} = \left(1 - \frac{\frac{1}{N}\sum_{n=1}^{N}(\alpha_n - \hat{\alpha}_n)^2}{\frac{1}{N}\sum_{n=1}^{N}(\alpha_n)^2}\right) \times 100 \tag{23}$$

where $\hat{\alpha}$ is the predicted output. Figure 9 shows a typical cross-validation output for the postulated ARMA model. The figure illustrates that a linear model is not capable of accurately reproducing the measured data with high accuracy. For all cross-validation datasets the ARMA model was only able to predict approximately 75% of the observed output variance. This result provides justification to assess whether a nonlinear model can provide improved predictive capability.

### B. Predicitive Capability Using a Nonlinear Model Formulation

We evaluated the ability of the nonlinear model given by Eqn. 20 to accurately predict the observed output. The parameterization chosen for the exponential terms, $p_2$ and $p_3$ is given in Table 2. The values of $p_2$ and $p_3$ were selected by trial and error as ones that provided good curve-fits with a maximum error of less than 10%. For estimation and model selection, we again used one output as estimation data and the remaining ten as validation data. A model (Eqn. 20) was estimated for each parameterization giving 16 models for every validation data record. Each model's output was computed using a $k$-step-ahead predictor and accuracy quantified as %Fit (Eqn. 23). The model that yielded the highest %Fit was deemed the best fit model. This procedure was repeated for each validation output.

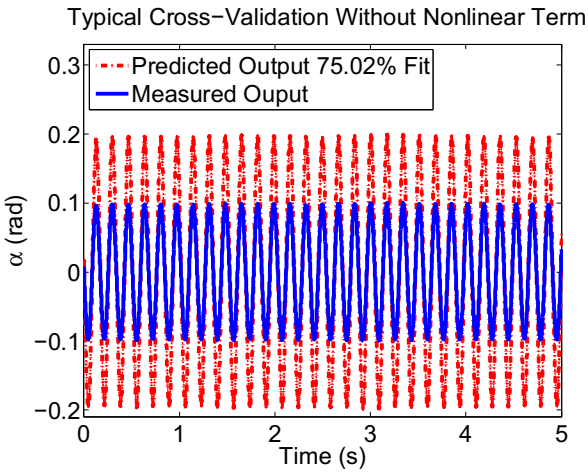


**Figure 9. Cross-Validation: Typical linear model prediction (dash-dot line "-.') superimposed on top of the measured output (solid-line "–").**

| | | | | | | | | | | | | | | | | |
|---|---|---|---|---|---|---|---|---|---|---|---|---|---|---|---|---|
| $p_2$ | 0.8 | 0.9 | 1.0 | 1.1 | 1.2 | 1.3 | 1.4 | 1.5 | 1.6 | 1.7 | 1.8 | 1.9 | 2.0 | 2.1 | 2.2 | 2.3 |
| $p_3$ | 0.1 | 0.2 | 0.3 | 0.4 | 0.5 | 0.6 | 0.7 | 0.8 | 0.9 | 1.0 | 1.1 | 1.2 | 1.3 | 1.4 | 1.5 | 1.6 |

**Table 2. Values of $p_2$ and $p_3$ used to parameterize the basis function in Eqn. 20.**

The results produced the same best fit model for each validation data indicating the estimated model is robust. The selected model was consistently parameterized with the values, $p_2 = 2.0$ and $p_3 = 1.3$.

Figure 10 provides a typical cross-validation output for the nonlinear model. The figure illustrates that this nonlinear model is capable of accurately reproducing the measured data with high accuracy. For all cross-validation datasets, the discrete-time nonlinear model was able to predict 99.2% of the observed output variance.

Figure 11 summarizes the cross-validation %Fit's for each validation data, The results show that the predicted output, for these parameter estimates, account for a large portion of the variance. This indicates that the model parameters explain the measured data well.

## VI. Discussion

Our results show that a linear model is not capable of reproducing the observed output for this model of stall flutter response. In many cases, researchers have not been able to quantify nonlinearities in their data, possibly due to it being collected about a small operating point, making the nonlinear effect unobservable.

Although our model is nonlinear, we posed a linear statistical model to implement a best fit model selection approach via cross-validation data to avoid using a nonlinear least-squares estimation approach. This approach was feasible due to having *a priori* insight to good parameterization (see Tab. 2) to be used with this model. Although this methodology provided a high percent fit for all validation sets, since the underlying model is nonlinear and we used a coarse parameterization, the estimated parameters may be at a local minimum. Nevertheless, the estimated model could be used in applications where the concern is to achieve high fidelity simulations or as a seeding in a nonlinear least-squares framework possibly facilitating rapid convergence to a global minimum.

In this study, we only considered one class of an infinite number of basis functions. It may be possible to reformulate this problem as a proper linear statistical model, thus, avoiding the need to have insight to "good" parameterization of the exponential term or other similar basis functions. In addition, recasting this problem in a linear framework offers the advantage of not converging to a local minimum. The results of this study will be presented in a future paper.

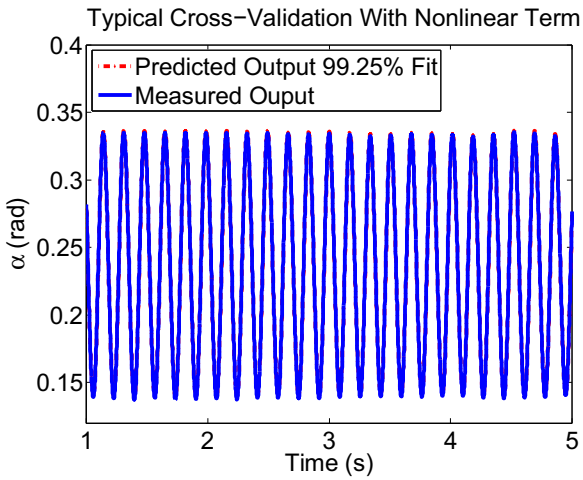


**Figure 10. Cross-Validation: Typical nonlinear model prediction (dash-dot line "-.') superimposed on top of the measured output (solid-line "–").**

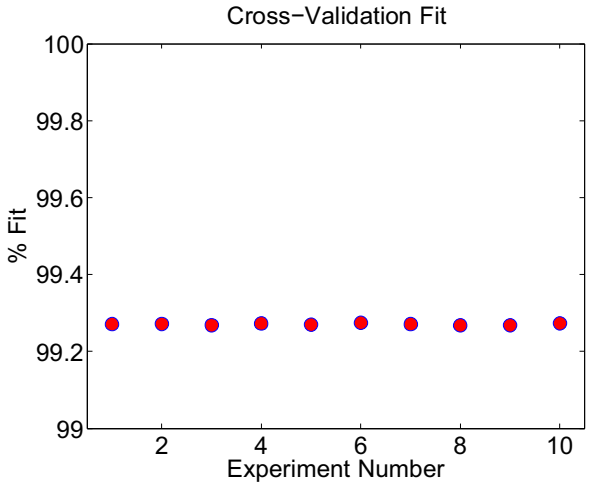


**Figure 11. Cross-validation: %Fit versus experimental trial.**

## VII. Conclusion

This study illustrates that nonlinear effects are present in the stall flutter response of an aeroelastic wing structure and that a nonlinear model is capable of modelling the dynamics with high accuracy. We showed that this nonlinear model can be accurately posed as a linear statistical model allowing $\ell_2$ estimation techniques to be used and, thus, avoiding a full nonlinear least-squares solution. These results may have utility for initialization of nonlinear least-square problems providing a global minimum in fewer steps than traditional approaches.

## References

[1]Dowell, E. H. and Tang, D., "Nonlinear Aeroelasticity and Unsteady Aerodynamics," *AIAA Journal*, Vol. 40, No. 9, 2002, pp. 1697–1707.

[2]Halfman, R. L., Johnson, H. C., and Haley, S. M., "Evaluation of high-angle-of-attack aerodynamic-derivative data and stall-flutter prediction techniques," Technical Note TN 2533, NACA, 1951.

[3]Fung, Y. C., *An Introduction to the Theory of Aeroelasticity*, Dover Publications, Inc., 1993.

[4]Parkinson, G., "Phenomena and modelling of flow-induced vibrations of bluff bodies," *Progress in Aerospace Sciences*, Vol. 26, No. 2, 1989, pp. 169–224.

[5]McCroskey, W. J., Carr, L. W., and McAlister, K. W., "Dynamic Stall Experiments on Oscillating Airfoils," *AIAA Journal*, Vol. 14, No. 1, 1976, pp. 57–63.

[6]Ericsson, L. E. and Reding, P. J., "Dynamic Stall at High Frequency and Large Amplitude," *Journal of Aircraft*, Vol. 17, No. 3, 1980, pp. 136–142.

[7]Spentzos, A., Barakos, G. N., Badcock, K. J., Richards, B. E., and McD. Galbraith, R. A., "Computational Fluid Dynamics Study of Three-Dimensional Dynamic Stall of Various Planform Shapes," *Journal of Aircraft*, Vol. 44, No. 4, 2007, pp. 1118–1128.

[8]Ericsson, L. E. and Reding, P. J., "Unsteady airfoil stall and stall flutter," Contractor Report CR 111906, NASA, 1971.

[9]Razak, N. A., Andrianne, T., and Dimitriadis, G., "Bifurcation analysis of a wing undergoing stall flutter oscillations in a wind tunnel," *Proceedings of the International Conference on Noise and Vibration Engineering, ISMA2010*, No. ISMA2010-0307, Leuven, Belgium, Sept. 2010.

[10]Abdul Razak, N., Andrianne, T., and Dimitriadis, G., "Flutter and stall flutter of a rectangular wing in a wind tunnel," *AIAA Journal*, Vol. 49, No. 10, 2011, pp. 2258–2271.

[11]Johansen, T. A. and Foss, B., "Identification of non-linear system structure and parameters using regime decomposition," *Automatica*, Vol. 31, No. 2, 1995, pp. 321–326.

[12]Johansen, T. A., "Identification of non-linear systems using empirical data and prior knowledge – an optimization approach," *Automatica*, Vol. 32, No. 3, 1996, pp. 337–356.

[13]Boulet, B. and Francis, B., "Consistency of Open-Loop Experimental Frequency-Response Data with Coprime Factor Plant Models," *IEEE Trans. Automatic Control*, Vol. 43, No. 12, 1998, pp. 1680–1691.

[14]Levenberg, K., "A Method for the Solution of Certain Non-Linear Problems in Least Squares," *The Quarterly of Applied Mathematics*, Vol. 2, 1944, pp. 164–168.

[15]Marquardt, D., "An Algorithm for Least-Squares Estimation of Nonlinear Parameters," *SIAM Journal on Applied Mathematics*, Vol. 11, No. 2, 1963, pp. 431–441.

[16]Morè, J., *The Levenberg-Marquardt algorithm: Implementation and theory*, Vol. 630 of *Numerical Analysis: Lecture Notes in Mathematics*, Springer-Verlag, New York, NY, 1978.

[17]Dimitriadis, G. and Li, J., "Bifurcation behavior of an airfoil undergoing stall flutter oscillations in a low speed wind tunnel," *AIAA Journal*, Vol. 47, No. 11, 2009, pp. 2577–2596.

[18]Li, J. and Dimitriadis, G., "Experimental study of stall-induced LCOs of free-vibrating wing," *Proceedings of the CEAS International Forum on Aeroelasticity and structural dynamics*, No. IF-026, Stockholm, Sweden, June 2007.

[19]Rae, Jr., W. H. and Pope, A., *Low Speed Wind Tunnel Testing*, John Wiley & Sons, New York, Chichester, Brisbane, Toronto, Singapore, 2nd ed., 1984.

[20]Strutz, T., *Data Fitting and Uncertainty: A Practical Introduction to Weighted Least Squares and Beyond*, Vieweg and Teubner, Wiesbaden, Germany, 2010.

[21]Ljung, L., *System Identification: Theory for the User*, Prentice Hall, Inc., Upper Saddle River, New Jersey, 2nd ed., 1999.